Numerical simulations of particle dispersion in an urban area

Emma Wingstedt and Bjørn Anders P. Reif

Norwegian Defence Research Establishment (FFI)

27 June 2012

FFI-rapport 2012/00266

1149

P: ISBN 978-82-464-2097-4
E: ISBN 978-82-464-2098-1

Keywords

Aerolsoler

Spredning

Deponering

Urbant miljø

CDF

Approved by

Monica Endregard	Project Manager
Jan Ivar Botnan	Director

English summary

In this study the transport and deposition of particles released from different source locations, and with different wind conditions, in a realistic urban area have been investigated. Two different scenarios have been considered. The first treats three point source locations at different heights with a wind velocity of 3 m/s. The second consider a moving source, representing a car driving at 30 km/h, with four different wind speeds (1 m/s, 3 m/s, 5 m/s and 10 m/s).

Results indicate a significant difference in horizontal dispersion when a source is placed above the building structures as compared to within. The dispersion from the roof yields a continuous cloud approximately 300 m wide, compared to a 150 m wide particle cloud when the source is below the roof tops. Also, more particles get deposited in the near field when released from within the urban area compared to a higher release point, and the higher the release point is located the more particles get deposited on buildings rather than on the ground.

It has also been shown that a higher wind velocity increased the vertical height of the plume as well as a wider horizontal dispersion pattern. There seems not to be any difference in the number of deposited particles, but they do however deposit differently. Therefore, for these two scenarios, the deposition pattern is more dependent on the source location, whereas the dispersion pattern is more dependent on the wind velocity.

Sammendrag

I denne studien har spredning og deponering av partikler, fra ulike kildeplasseringer og med ulike vindhastigheter, i et realistisk urbant område blitt undersøkt. To ulike scenarioer er blitt vurdert. Det første behandler tre punktkilder plassert i ulike høyder og med en vindhastighet ($3\ m/s$). Det andre beskriver en bevegelig kilde, som representerer en bil som kjører i $30\ km/t$, og fire forskjellige vindhastigheter ($1\ m/s$, $3\ m/s$, $5\ m/s$ og $10\ m/s$).

Resultatene indikerer en betydelig forskjell i horisontal spredning når en kilde er plassert over bygningene i forhold til mellom bygningene. Flere partikler blir deponert når de slippes nærmere bakken sammenlignet med et utslipp fra en høyere posisjon. Det kan også observeres at flere partikler blir deponert på bygninger i forhold til bakken når kildeplasseringens avstand til bakken øker.

Det har også blitt vist at en høyere vindhastighet både resulterer i en mer vertikalt utbredd sky og et bredere horisontalt spredningsmønster. Det ser ikke ut til å være noen betydelig forskjell i antall deponerte partikler i nærfeltet ($< 500\ m$), men deponeringsmønstret er annerledes. Denne studien indikerer derfor at deponeringen avhenger mer av kildens plassering enn av vindhastigheten, men at spredningen er mer påvirket av vindstyrken.

Contents

Preface

Visualizations of the simulations presented in this report can be obtained by contacting the Protection Division at the Norwegian Defence Research Establishment.

1 Introduction

Release and dispersion of hazardous materials in populated urban areas, whether it is a result of an accident or a planned attack, is of great concern to both authorities and military personnel. Identifying appropriate protective and emergency response measures against the effects of such incidents is an important area of research. It is however imperative that a physically sound approach is utilized in order to present the end-users with a realistic estimate of the spatial and temporal development of the dispersed plume of hazardous materials. Many hazardous materials are dispersed in the form of particles (or aerosols). In this study we have focused on release and dispersion of particles in a realistic urban environment.

In urban environments the dominating effects on the flow field are kinematic blocking of velocity components normal to solid surfaces and non-local effects caused by pressure reflections (cf. e.g.,(Durbin and Reif, 2002)). The non-local effects dominate in the atmospheric boundary layer (ABL) where they modify the turbulence anisotropy yielding a change in the dispersion process. The kinematic blocking dominates the local flow conditions in built up areas, where buildings cause street canyon effects, flow separation and generation of unsteady wakes. On top of this is the incoming atmospheric boundary later that can reach depths of 300 - 500 meters depending on the global weather conditions. This boundary layer also carries three-dimensional and time varying large scale structures that efficiently mix a dispersed contaminant. The local urban wind field thus comprises a continuous range of spatial and temporal scales mainly generated by velocity shear caused by a large number of different processes.

Due to a steadily increasing computer capacity, Computational Fluid Dynamics (CFD) has become a more popular tool for modeling dispersion. However, a number of modeling issues need to be addressed in order to warrant the use of CFD in urban areas (Lee et al., 2000). Many urban dispersion studies are based on the assumption that the flow field is statistically steady, and therefore the steady state Reynolds-averaged Navier-Stokes (RANS) method is widely used (see e.g.,(Coirier et al., 2005; Lien and Yee, 2004; Lien et al., 2006; Santiago et al., 2007)). Results show that even though the mean velocity field can be fairly well predicted with this method, the turbulence kinetic energy is in general underpredicted, which may lead to poorly predicted mixing processes. A number of studies regarding numerical simulation of particle dispersion using the Unsteady RANS (URANS) approach have also been carried out in the past (Wingstedt and Reif) with fairly good results. The URANS method inherently assumes the mean flow field to be statistically unsteady, an assumption better suited for flow in an urban environment due to bluff body shedding downstream building structures.

The primary objective of this study is to conduct a comparative assessment of the effect of different source types, and locations, as well as wind velocities on the resulting dispersion- and deposition-patterns of particles in an urban environment. This objective is reached by employing the more accurate URANS approach in conjunction with a Lagrangian description of the particle trajectories explicitly taking into account the particle size, mass, and inertia.

2 Source description

Two different types of sources have been considered. The first type is stationary sources with release times significantly longer than the local wind field time scale such that these can be characterized as continuous sources. The second class is a source moving with a constant velocity which is comparable to the wind field velocities considered here (approximate ~ 8 m/s). This implies that although the moving source releases particles with a constant flux, it cannot be considered as continuous release since the local release time (L/U_{source}) is of the same order as the wind field time scale, *i.e.,* the large scale turbulence time scale τ. The implication of this difference is mainly related to the effectiveness of the streamwise dispersion processes (the dispersion in the wind field direction). In both cases the released plume will experience a strong turbulent mixing in the directions normal to the wind direction. However, the latter non-continuous release (sometimes referred to as a "puff" release) will in addition experience a significant mixing also in the streamwise direction resulting in lower concentration levels (Durbin, April 1983). The two above mentioned scenarios are hereafter referred to as (i) the hotel scenario and (ii) the car scenario.

In the hotel scenario, particles are released from three different point sources located at ground level, 10 meter above ground which represents a window, and at a roof top 22 meters above ground, respectively. From all sources the particles are released with a velocity of 3 m/s in the wall-normal direction, *i.e.,* in vertical upward direction when the release is from ground level and roof top, and in the horizontal outward direction from a window (see Fig.4.1). The global wind velocity is set to be 3 m/s in the y-direction as shown in Figure 4.1. The releases are continuous for 30 s, during which 20000 particles are continuously discharged. The particles have the same density as liquid water, and their diameters are specified to vary linearly between 1 and 50 μm. This corresponds to a variation of the global averaged Stokes number, $St \equiv \tau_p/\tau$ where τ_p is the particle relaxation time, of $1.8 \cdot 10^{-5} \leq St \leq 5 \cdot 10^{-2}$. It should be noted that the Stokes number varies throughout the domain although the particle diameter remains constant. The reason for this is that the turbulent time scale τ depends on the local flow field and therefore varies in space and time.

The car scenario comprises of a source moving along the red line in Figure 4.1 with a constant velocity of 30 km/h. The released particles have the same physical properties and size ratio as in the hotel scenario. The particle flux is constant and equal to 335 particles/second during a 83.4 seconds release (*i.e.,*the total number of released particles is 28000). The release is directed vertically (upwards) with a velocity of 3 m/s, but it also has horizontal components corresponding to the speed (30 km/h) and direction of the moving source, which vary in the domain. In order to investigate the influence of the global wind speed this scenario has been simulated with four different wind velocities, 1 m/s, 3 m/s, 5 m/s, and 10 m/s.

3 Mathematical modeling

The equations governing the conservation of the mass and ensemble averaged (mean) momentum for a Newtonian, incompressible fluid are given by the RANS equations that can be written as

$$\frac{\partial U_i}{\partial x_i} = 0 \tag{3.1}$$

$$\frac{\partial U_i}{\partial t} + U_j \frac{\partial U_i}{\partial x_j} = -\frac{1}{\rho}\frac{\partial P}{\partial x_i} + \frac{\partial}{\partial x_j}\left[\nu \frac{\partial U_i}{\partial x_j} - \overline{u_i' u_j'}\right] + g_i \tag{3.2}$$

where $P(\mathbf{x}, t)$ and $U_i(\mathbf{x}, t)$ represent the mean pressure and the mean velocity in the x_i-direction respectively. ρ denotes the density, ν the kinematic viscosity, and g_i is the gravitational acceleration in the x_i-direction. The unclosed term in Eq.(3.2), $\overline{u_i' u_j'}(\mathbf{x}, t)$, is the Reynolds stress tensor, which physically represents the average effect of turbulence on the mean flow field. This term needs to be modeled in order to close the RANS equations. Here, the generalized Boussinesq hypothesis has been used which is a constitutive relation that relates turbulent stresses linearly to the mean strain rate

$$\overline{u_i' u_j'} = \frac{2}{3} k \delta_{ij} - \nu_t \left(\frac{\partial U_i}{\partial x_j} + \frac{\partial U_j}{\partial x_i}\right). \tag{3.3}$$

Here $k \equiv \frac{1}{2}\overline{u_i' u_i'}$ is the turbulence kinetic energy and δ_{ij} is the Kronecker delta. It should be noted, however, that this simple algebraic formula lacks the ability to represent temporal relaxation effects. That is, it inherently assumes an instantaneous equilibrium between $\overline{u_i' u_j'}$ and the mean flow field; if the mean flow field changes due to e.g.,pressure-gradient effects, the turbulence field is assumed to instantaneously respond to this change. This drawback is however believed to be of less importance in the present case, since the mean flow field is not statistically steady; the unsteadiness of the mean flow field is a significant contributor to the mixing processes taking place in the wind field. This drawback is significantly more severe in cases with a statistically steady background wind field (such as the wind field over flat terrain).

3.1 Realizable $k - \varepsilon$ model

The realizable $k - \varepsilon$ model of (Shih et al., 1995) has been used in this study. The term "realizable" is used since the realizability constraints

$$\begin{aligned} &(i) && \overline{u_\alpha'^2} \geq 0, \\ &(ii) && \overline{u_\alpha'^2} \leq 2k, \\ &(iii) && \left(\overline{u_\alpha' u_\beta'}\right)^2 \leq \overline{u_\alpha'^2}\,\overline{u_\beta'^2}, \end{aligned}$$

were applied to derive the functional form of the coefficient C_μ (cf. Eq.(3.6)). Here $\alpha, \beta = 1, 2, 3$. Realizability is a mathematical constraint derived from the properties of $\overline{u_i' u_j'}$ which makes it physically consistent with some limiting states of turbulent flows. The last constraint, (iii), is the so-called Schwartz inequality.

The modeled transport equations for the turbulence kinetic energy and its rate of viscous dissipation

can be written as

$$\frac{\partial k}{\partial t} + U_i \frac{\partial k}{\partial x_i} = \nu_t \left[\left(\frac{\partial U_i}{\partial x_j} + \frac{\partial U_j}{\partial x_i} \right) \frac{\partial U_i}{\partial x_j} \right] - \varepsilon + \frac{\partial}{\partial x_j} \left[\left(\nu + \frac{\nu_t}{\sigma_k} \right) \frac{\partial k}{\partial x_j} \right], \tag{3.4}$$

and

$$\frac{\partial \varepsilon}{\partial t} + U_i \frac{\partial \varepsilon}{\partial x_i} = \frac{\partial}{\partial x_j} \left[\left(\nu + \frac{\nu_t}{\sigma_\varepsilon} \right) \frac{\partial \varepsilon}{\partial x_j} \right] + C_1 \varepsilon S - C_2 \frac{\varepsilon^2}{k + \sqrt{\nu \varepsilon}}, \tag{3.5}$$

respectively, where

$$C_1 = max \left[0.43, \frac{S k \varepsilon^{-1}}{\varepsilon k^{-1} S^{-1} + 5} \right], \qquad S = \sqrt{2 S_{ij} S_{ij}}.$$

and

$$C_2 = 1.9, \quad \sigma_k = 1.0, \quad \sigma_\varepsilon = 1.2.$$

The turbulent kinematic viscosity in Eq.(3.3) is calculated as

$$\nu_t = \underbrace{(A_0 + A_s \xi)^{-1}}_{C_\mu} \frac{k^2}{\varepsilon}, \tag{3.6}$$

$$\xi = \varepsilon^{-1} k U^* = \varepsilon^{-1} k \sqrt{S_{ij} S_{ij} + \Omega_{ij} \Omega_{ij}} \tag{3.7}$$

where C_μ is a function of the mean strain and rotation rates. The model coefficients, A_0 and A_s, can be found in (Shih et al., 1995).

3.2 Particle Transport Modeling

Particle transport is modeled using a discrete phase model, which determines the particle trajectory by integrating the force balance on the particle written in a Lagrangian reference frame. The force balance can be written as

$$\frac{dU_p}{dt} = F_D (U - U_p) + \frac{g_i (\rho_p - \rho)}{\rho_p} + F_x \tag{3.8}$$

where U_p and U are the particle and fluid velocity, respectively. F_D is the drag force on the particle exerted by the wind field, and ρ and ρ_p denote the fluid and particle densities, respectively. The term F_x incorporates the force that arises due to the pressure gradients and virtual mass, *i.e.,*

$$F_x = \left(\frac{\rho}{\rho_p} \right) U_{p,i} \frac{\partial U}{\partial x_i} + \frac{1}{2} \frac{\rho}{\rho_p} \frac{d}{dt} \left(U - U_p \right). \tag{3.9}$$

The drag force is modeled using a spherical drag

$$F_D = \frac{18 \mu}{\rho_p d_p^2} \frac{C_D Re}{24}. \tag{3.10}$$

Here, d_p is the particle diameter, Re is the slip-velocity Reynolds number defined as $Re \equiv \mu^{-1}\rho d_p|U_p - U|$, C_D is the drag coefficient, and μ is the molecular viscosity of the fluid. In this study we use $C_D = a_1 + a_2 Re^{-1} + a_3 Re^{-2}$. The constants a_1, a_2 and a_3 apply to smooth spherical particles over a wide range of slip-velocity Reynolds numbers.

From Eq.(3.8) the displacement of particles is only dependent on the mean fluid velocity. In order to account for random fluctuations due to the turbulence field a stochastic tracing model is applied, through which a fluctuating velocity component is added. These fluctuations are discrete piecewise constant functions of time and their random value is kept constant over an interval of time given by the characteristic life time of the eddies ($\sim k/\varepsilon$). It should finally be noted that the particle concentration at any given time is assumed to be diluted, *i.e.,* the effect of the particle on the flow field is neglected.

4 Numerical approach

4.1 Mesh generation

A central part of Oslo city is chosen as computational domain to assess the particle dispersion in a realistic urban area (see Fig.4.1).

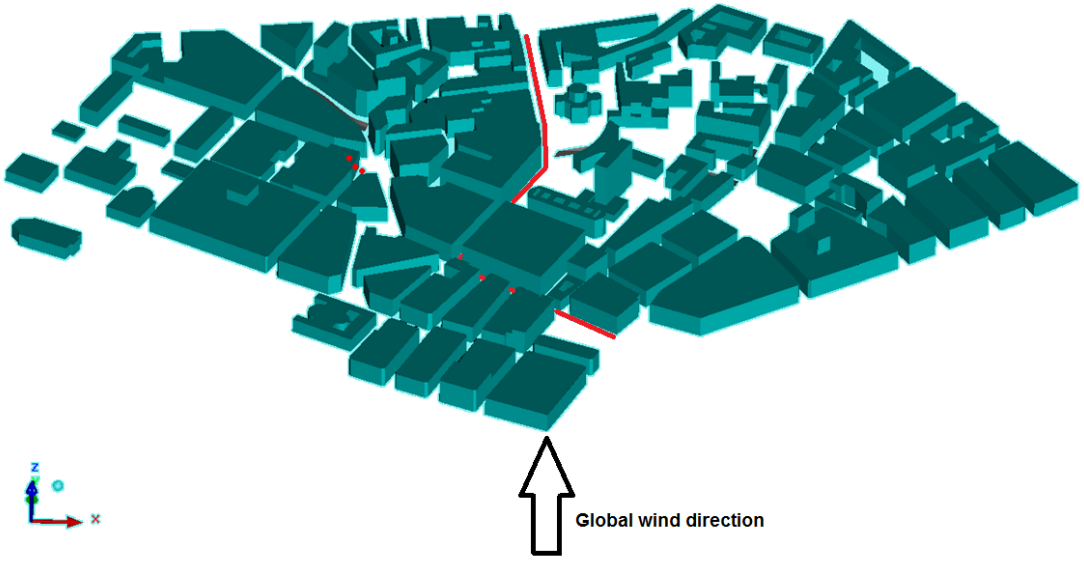

Figure 4.1 *An overview of the computational domain with dimensions* 1300 *x* 900 *x* 300 m^3. *The red dots show the stationary sources, and the red line represents the moving source.*

The area, in total 1300 x 900 x 300 m, is discretized into approximately $75 \cdot 10^6$ cells, where the smallest cells (approximately 6 x 6 x 6 cm^3) are located in close proximity of the release points (see Figure4.2).

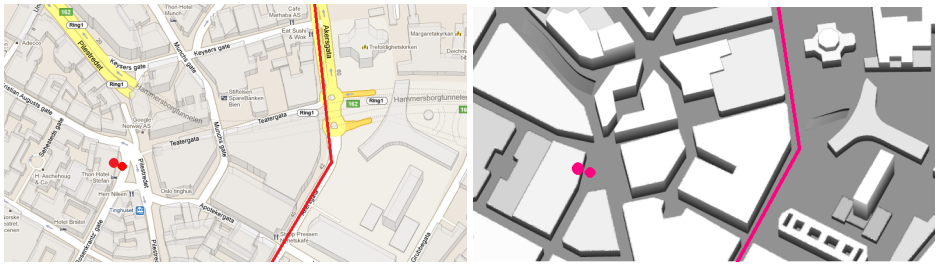

Figure 4.2 *Source location on map and in the geometry. The red dots show the stationary source locations, and the red line represents the moving source.*

In the computational domain, it is assumed to be no elevation in ground level. Also, buildings lower than $5\ m$ have been disregarded, and some blocks are simplified to be a single building. Due to the large computational domain, we do not expect to get grid independent solutions.

4.2 Boundary conditions

In the simulations, the global wind direction is in the y-direction (see Fig. 4.1). In order to obtain realistic inlet boundary layer profiles, steady state simulations using constant velocities of $1\ m/s$, $3\ m/s$, $5\ m/s$ and $10\ m/s$ were first conducted and the results, in terms of velocity components as well as turbulence quantities were used as an input plane for the remaining simulations. The outlet boundary is defined as a pressure outlet, allowing particles to pass through, and at the top and lateral boundaries of the computational domain, symmetry conditions with escape possibilities for the particles are prescribed. All the symmetry boundaries are sufficiently far away from the area of interest so that any influence of the symmetry assumption is negligible on the solution. Both the ground and all of the building surfaces are defined as no-slip walls, which trap discrete particles.

A time step corresponding to an estimate of the time scale for the large scale turbulence, *i.e.*, $\Delta t = \tau = L/U = 0.3\ s$, is used.

5 Computational results

In the following section, results from the stationary source as well as the moving source will be evaluated.

5.1 Stationary source

In the hotel scenario, the main interest is to investigate possible effects of different source locations on the dispersion and deposition processes.

Figure 5.1 shows how the particles from the different sources are dispersed at different times. It is seen that the release from ground level (red particles) and the release from a window (white particles) are transported in quite the same manner. After $90\ s$ it is difficult to separate the two. The

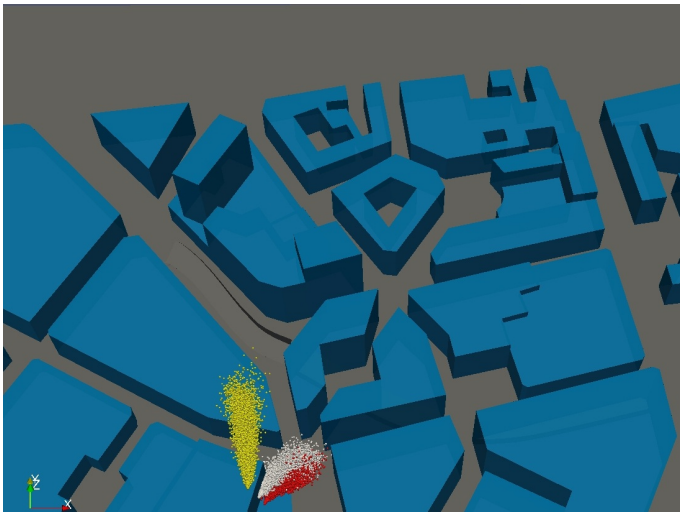

(a) $t = 30\ s$

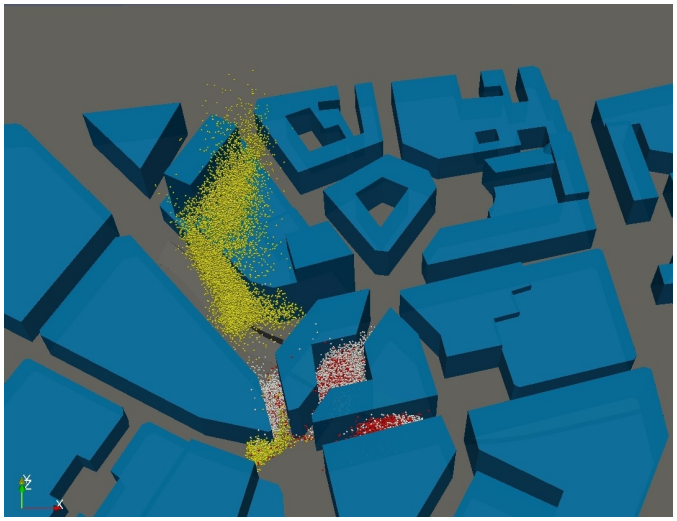

(b) $t = 90\ s$

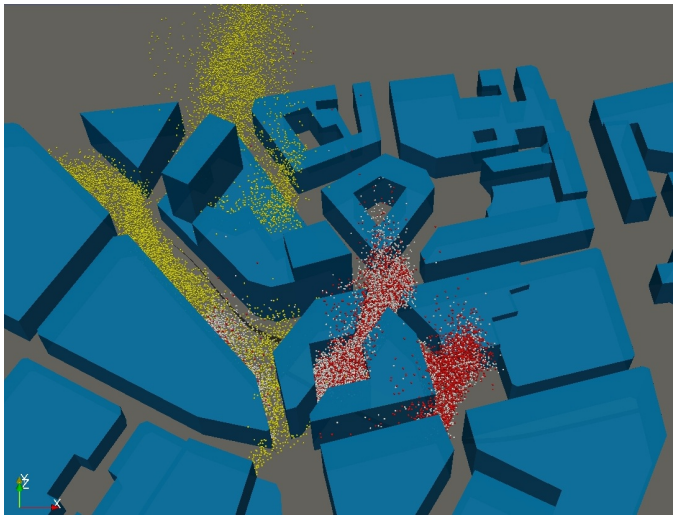

(c) $t = 150\ s$

Figure 5.1 *Particle dispersion from three different sources at different instances in time. Yellow particles are released from a roof, white particles from a window and red particles from the ground.*

particles released above the buildings (yellow particles) are less affected by the building structures and get a quicker transport compared to the lower source locations. However, it is also seen that many of the yellow particles are dispersed within the street canyons.

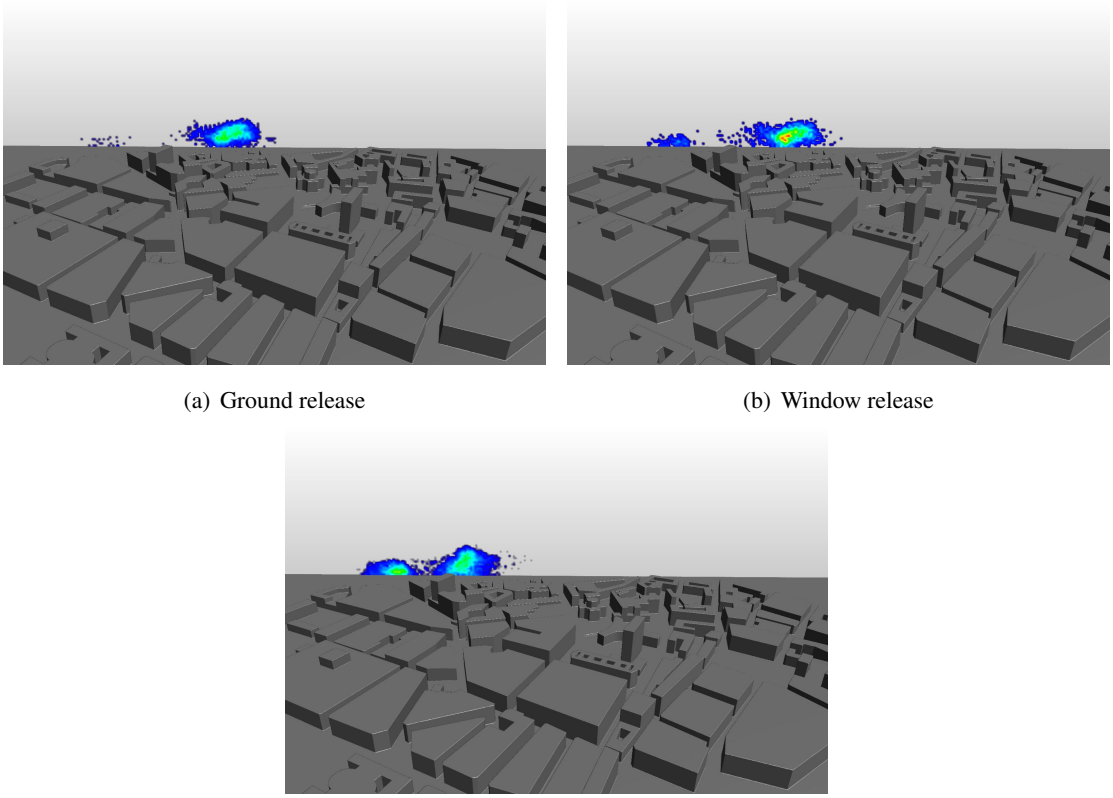

(a) Ground release

(b) Window release

(c) Roof top release

Figure 5.2 Particle dispersion from three different sources after $450\ s$.

Figure 5.2 shows particle concentration plots on a vertical plane located approximately $370\ m$ from the release for the different source locations; from the ground (Figure 5.2(a)), window (Figure 5.2(b)) and roof (Figure 5.2(c)). The maximum concentration, i.e., the color red in the figures, correspond to 4 particles per m^2. The dispersion pattern is quite similar, especially between the ground and window release. In total, the concentration cloud from the roof top release is approximately $15\ m$ higher than the cloud from the ground release. The height difference between these two sources was $21\ m$. There is however a bigger difference in the horizontal dispersion when comparing the different sources. Release from above the building yields a continuous cloud, approximately $300\ m$ wide.

Particles deposited on the ground and on buildings after $450\ s$ can be seen in Figure 5.3. Here, red particles are released from ground level, white from a window and the yellow particles from a roof top. Again, it is seen that the patterns between ground and window release are quite similar, while

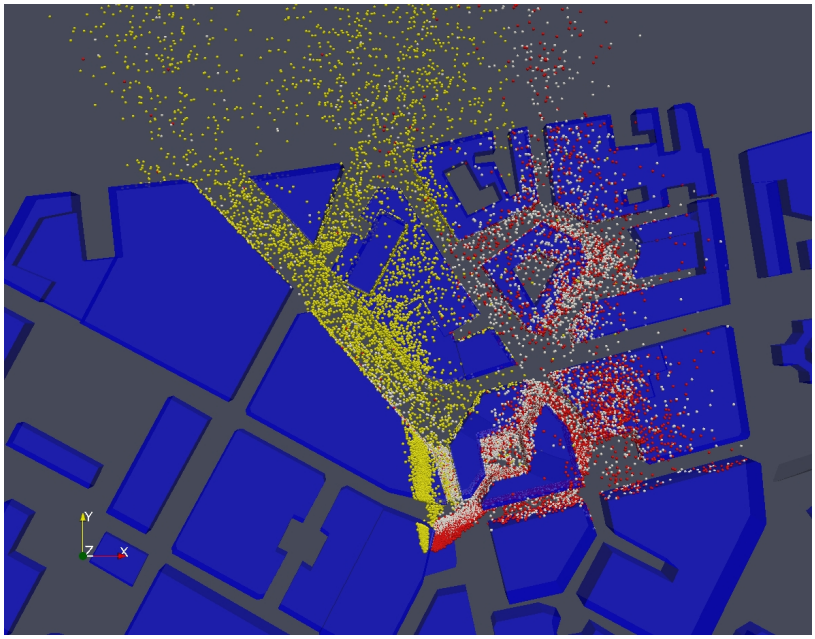

Figure 5.3 *Deposited particles from three different sources after* $450\ s$. *Red particles are released from ground level, white particles from a window, and the yellow particles from a roof top.*

the roof top release yields a wider deposition pattern.

To investigate if there is a difference in deposition depending on source location, deposited particles in time are plotted in Figure 5.4. In the top figure, showing particles deposited on the ground, it is seen a big difference in the number of deposited particles depending on the source location. After $450\ s$, 15% of the particles released from the roof have deposited on the ground. In the same time, approximately 47% of the particles released from ground level are deposited. It is also noticeable that it takes almost one and a half minute before particles from the roof starts to deposit on the ground. The bottom figure shows particles deposited on the buildings and an opposite trend can be seen; the higher the source is located, the more particles are deposited. Again, there is a lag in when the particles start to deposit, but this time for the ground level release. By adding the information from both figures, it is established that approximately 57% of all released particles from the roof are deposited, 75% of all released particles from the window are deposited and 78% of all released particles from the ground are deposited. Hence, the biggest difference in transport and deposition are between the sources located within the building structures compared to the one source above the buildings.

5.2 Moving source

In this scenario the source was moving with a constant speed, representing a car driving down the street without stopping while continuously releasing particles. Simulations using four different wind velocities with the same source characteristics have been carried out, and the resulting dispersion-

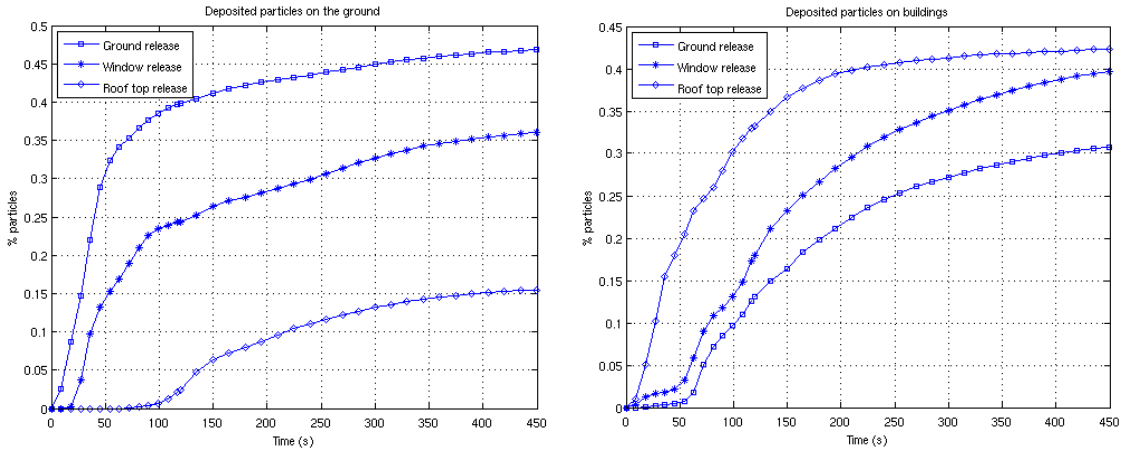

(a) Ground deposition

(b) Building deposition

Figure 5.4 Particle deposition in time. Fraction of deposited particles to the total number of released particles.

and deposition patterns are presented here.

Figure 5.5 shows the particle dispersion with a wind velocity of 3 m/s at three different instances in time; when the car stops after driving approximately 685 m with a velocity of 30 km/h, 60 s after the car stops moving, and finally 120 s after the car stops moving. From the above figure, it is seen that even though more than a minute has passed since the car was at its starting position, most particles are in close proximity to where they were released. As time passes, the particles get more dispersed, but they mostly follow the streets even if that means transport against the global wind direction. This is due to the street canyon effects.

Particle concentration on a vertical plane located approximately 115 m downwind the starting position of the vehicle, after 750 s, with four different wind velocities can be seen in Figure 5.6. A difference in height between the clouds depending on wind speed is noticeable; 1 m/s wind yields approximately a 55 m high plume, while the 10 m/s wind gives a 100 m high cloud. More interesting is how the spanwise dispersion increases as the wind speed increases. There is a difference of almost 600 m in the lateral spread of particles between the highest and the lowest wind velocities.

Figure 5.7 shows the particles deposited on both the ground and the buildings after 750 s. Here, white particles represent a wind speed of 1 m/s, red represent 3 m/s, yellow 5 m/s and the green particles are simulated using a wind velocity of 10 m/s. Even though there was a big difference in the dispersion pattern on the outlet of the domain, the deposition patterns seem to correspond quite well, and it is difficult to spot any differences depending on wind velocity.

The positions where the particles get deposited and how deposition distribution varies in time are shown in Figure 5.8. The top plot illustrates the ground deposition. It is apparent that during the release, *i.e.,* for the first 82 s, the effect of the wind speed is insignificant. When the release has stopped, the velocity of the wind starts to influence; a lower velocity yields a higher particle

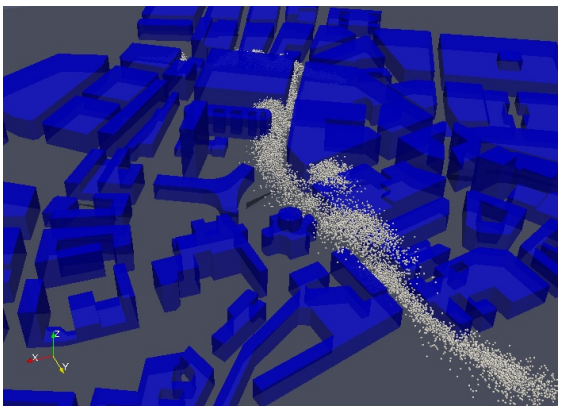

(a) Car stops releasing particles

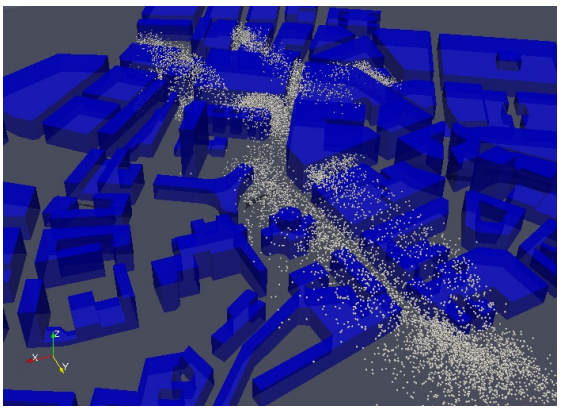

(b) 60 s after the car stops releasing particles

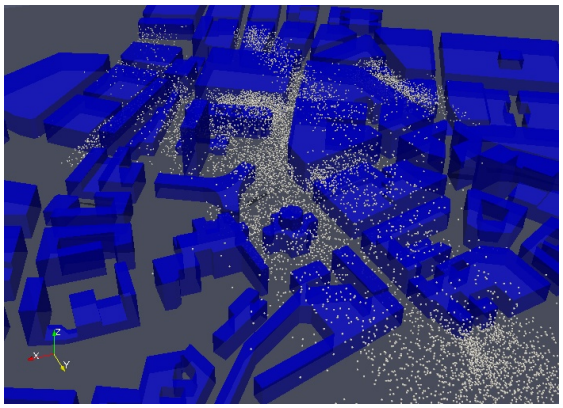

(c) 120 s after the car stops releasing particles

Figure 5.5 *Particle dispersion from a moving source at different instances in time. The global wind velocity is* 3 m/s *and in the* y*-direction (i.e., from upper left to lower right corner)*

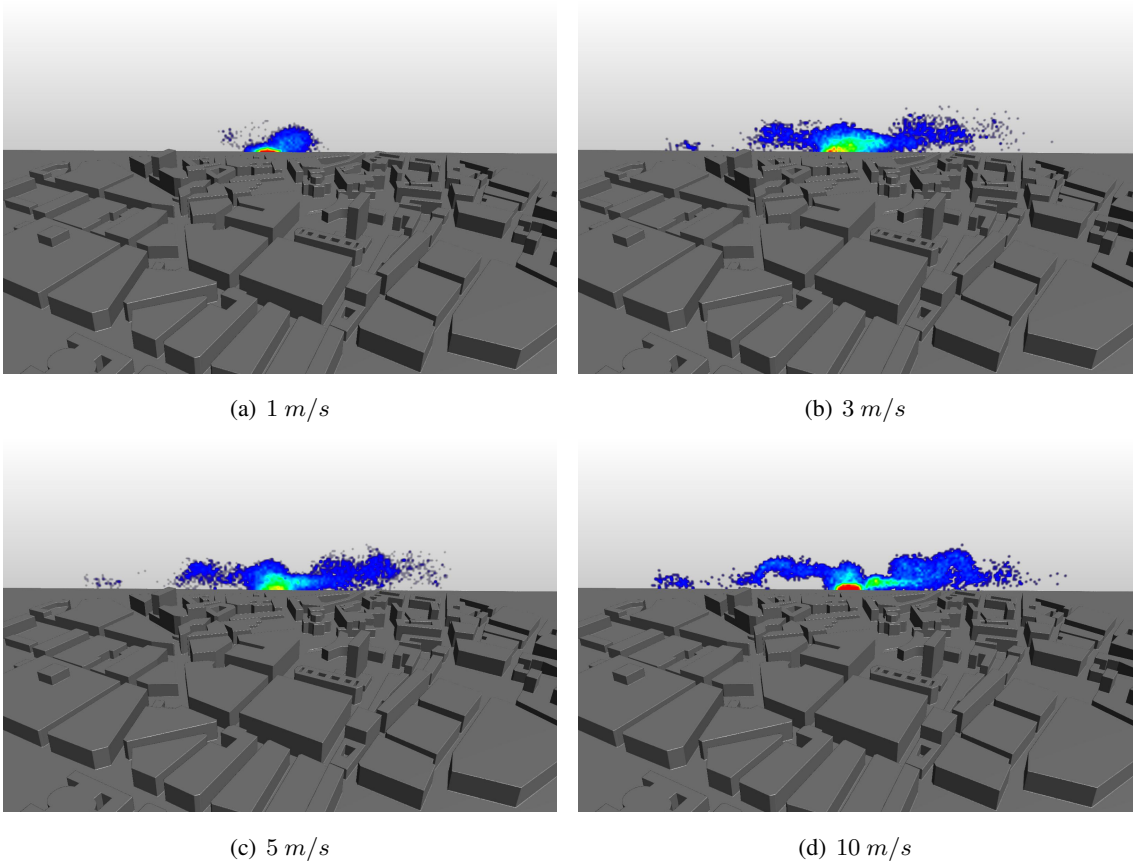

(a) $1\ m/s$ (b) $3\ m/s$

(c) $5\ m/s$ (d) $10\ m/s$

Figure 5.6 Particle dispersion from a moving source with four different wind speeds after $750\ s$

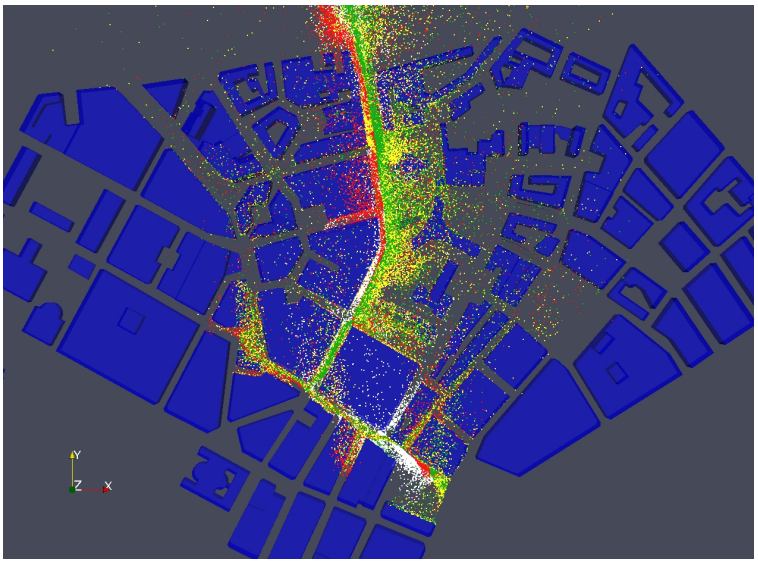

Figure 5.7 Deposited particles with four different wind speeds after $750\ s$*. White particles are simulated with a wind speed of* $1\ m/s$*, red with* $3\ m/s$*, yellow with* $5\ m/s$ *and the green particles are with* $10\ m/s$*.*

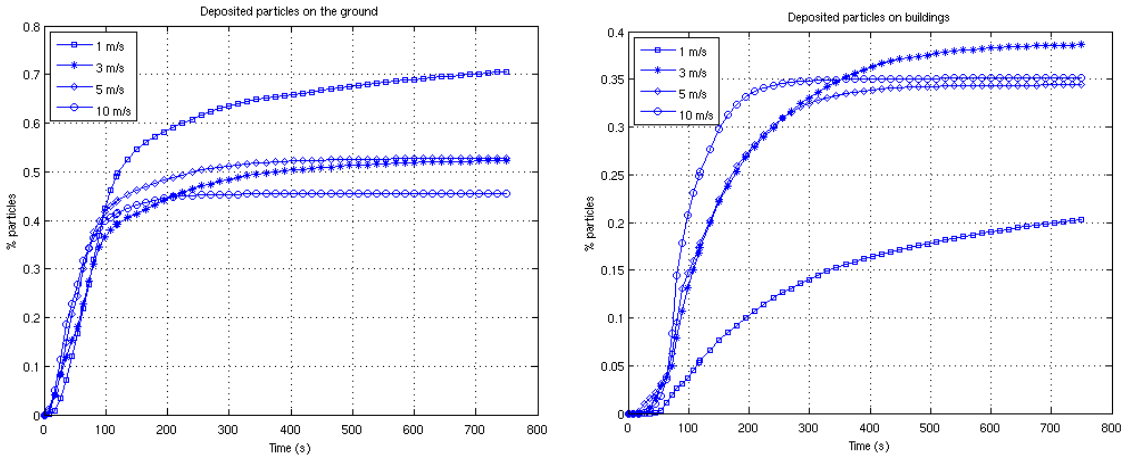

(a) Ground deposition

(b) Building deposition

Figure 5.8 *Particle deposition in time. Fraction of deposited particles to the total number of released particles.*

deposition on the ground. Also, after approximately 200 s the particles influenced by a wind speed of 10 m/s stop being deposited on the ground, whereas the particles affected by the 1 m/s wind keep getting deposited during the entire simulation. In the lower figure it is seen that higher wind speed gives more deposited particles on the buildings. It is however not a significant difference as long as the wind is stronger than 3 m/s. In total, the number of deposited particles varies between approximately 80% and 90% depending on the wind, but the difference lies in where they are deposited. Hence, it seems like the location of the source is of more importance than the wind speed when it comes to deposition.

6 Concluding remarks

The main focus of this study was to conduct a comparative assessment of the effects of different source locations and wind velocities on dispersion and deposition patterns of particles released within a realistic urban environment. For this reason two different scenarios have been investigated, one with a stationary source at different heights and the same wind velocity and the second with a moving source and four different wind forces. The results have shown that the location of the source is of most importance for both dispersion and deposition. A significant difference, especially in deposition of particles, is observed when placing the source above the building structures compared to within. It has also been shown that a higher wind velocity gives both a higher plume as well as a wider horizontal dispersion pattern. The number of deposited particles is, however, almost the same, but they get deposited differently in the geometry. Therefore, for these two scenarios it seems like the deposition varies more depending on the source location, while the dispersion pattern is more affected by the wind force.

References

W. J. Coirier, D. M. Fricker, M. Furmanczyk, and S. Kim. A Computational Fluid Dynamics approach for urban area transport and dispersion modeling. *Environmental Fluid Dynamics*, 5: 443–479, 2005.

P. A. Durbin. Stochastic differential equations and turbulent dispersion. *NASA Reference Publication*, 1103, April 1983.

P. A. Durbin and B. A. Petterson Reif. The elliptic relaxation method. In B. Launder and N. Sandham, editors, *Closure Strategies for Turbulent and Transitional Flows*. Cambridge University Press, 2002. ISBN 0 521 79208 8.

R. L. Lee, R. J. Calhoun, S. T. Chan, J. Leone, J. H Shinn, and D. E. Stevens. Urban dispersion CFD modeling, fact or fiction? In *84th AMS meeting, 3rd Symposium on the Urban Environment*, Davis, CA, USA, 2000.

F.-S. Lien and E. Yee. Numerical modelling of the turbulent flow developing within and over a 3d building array, part i: A high-resolution Reynolds-Averaged Navier-Stokes approach. *Boundary-Layer Meteorology*, 112:427–466, 2004.

F.-S. Lien, E. Yee, H. Ji, A. Keats, and K. J. Hsieh. Progress and challenges in the development of physically-based numerical models for prediction of flow and contaminant dispersion in the urban environment. *Int. Journal of Computational Fluid Dynamics*, 20:323–337, 2006.

J. L. Santiago, A. Martilli, and F. Martin. Cfd simulation of airflow over a regular array of cubes. part i: Three-dimensional simulation of the flow and validation with wind-tunnel experiments. *Boundary-Layer Meteorology*, 122:609–634, 2007.

T. H. Shih, W. W. Liou, A. Shabbir, Z. Yang, and J. Zhu. A new $k - \epsilon$ eddy-viscosity model for high reynolds number turbulent flows - model development and validation. *Computers Fluids*, 24, 1995.

E. M. M. Wingstedt and B. A Pettersson Reif. Statistically unsteady mixing and its effect on urban disperison of particles. *Submitted to Boundary-Layer Meteorology*.